Zero : Jurnal Sains, Matematika, dan Terapan
E-ISSN : 2580-5754; P-ISSN : 2580-569X
Volume 9, Number 2, 2025
DOI: 10.30829/zero.v9i2.25942
Page: 555-564

Oil Spill Detection and Verification in Nothern Bintan

[1] **Brigitta Aurelia Putri Suhendi**
Department of Statistical Computing, Politeknik Statistika STIS, Jakarta, Indonesia

[2] **Waris Marsisno**
Department of Statistical Computing, Politeknik Statistika STIS, Jakarta, Indonesia

Article Info

Article history:

Accepted, 30 October 2025

Keywords:

Look-alike;
Machine Learning;
Oil Spill;
Radar Satellite Imagery.

ABSTRACT

The Riau Islands Province, particularly northern Bintan Island, is strategically located near countries such as Singapore, making it a gateway to regional and international markets but also vulnerable to oil spills. This study aims to detect oil spill areas using GLCM texture analysis, adaptive thresholding, and various machine and deep learning models, followed by look-alike verification. The XGBoost model achieved the best performance with an accuracy of 0.9772, detecting oil spill areas of 5,400,241 m² and look-alike regions covering 1,333,045 m² on March 23, 2024. The findings also indicate that inland waters are often misidentified as spills, highlighting the importance of verification. This study is the first to integrate several of these methods for Sentinel-1 based oil spill detection in Bintan waters, as a new approach to accurate and efficient regional monitoring.

Corresponding Author:

Brigitta Aurelia Putri Suhendi,
Department od Statistical Computing
Politeknik Statistika STIS, Jakarta, Indonesia
Email: putriaurelia228@gmail.com

1. INTRODUCTION

The Riau Islands Province holds a strategic position as a center of trade and maritime activity due to its location stretching from the Malacca Strait to the South China Sea and its proximity to countries such as Singapore and Malaysia. Among its 2,408 islands, Bintan Island is the largest and serves as a key area for economic and tourism development. However, its position along major shipping routes also makes it highly vulnerable to marine pollution, particularly oil spills from tanker, commercial, and passenger ship activities [1].

Oil spills have a significant impact on national development. Based on Green Theory in international relations, environmental pollution can influence a country's development through its economy. Such environmental pollution can take the form of oil spills, which can cause losses in the economic sector, especially in the tourism, fisheries, and trade sub-sectors [2]. To that end, the government formed the National Oil Spill Emergency Response Team through Presidential Regulation No. 109 of 2006, with the Directorate of Pollution and Environmental Damage Control of the Ministry of Environment and Forestry tasked with following up on reports of oil spills [3], [4], [5]. However, in practice, this directorate still does not have complete daily oil spill data [6], [7].

This data incompleteness can be addressed through advanced technology–based environmental monitoring systems, one of which utilizes Sentinel-1 radar satellite imagery. Sentinel-1 is particularly effective because it can capture images both day and night under all weather conditions, making it highly reliable for continuous monitoring in maritime regions [8]. However, the detection process can face obstacles in the form of look-alike objects such as natural surfactants, rainfall, or areas with low wind speeds, which may resemble oil spills. To overcome these challenges, the integration of multi-source data and the application of machine learning models offer promising solutions, as they can improve detection accuracy by distinguishing true oil spills from look-alike

phenomena [9]. This study utilizes Sentinel-1 imagery for daily detection of oil spills in the waters north of Bintan Island, then builds the best detection model from machine learning and deep learning, and identifies look-alikes using ECMWF wind data, UCSB/CHG rainfall, NOAA sea temperature, and Google Street View.

Research related to oil spill detection has been conducted previously, for example by Prastyani & Basith (2019) in the Makassar Strait using radar and optical imagery with visual interpretation methods [9], and by Najafizadegan & Danesh-Yazdi (2023) using CNN algorithms [10]. However, to date, no research has been found that combines texture analysis, adaptive thresholding, and machine learning or deep learning models to detect oil spills, particularly in northern Bintan Island, as well as look-alike identification based on multi-source data. Thus, this study is expected to contribute to filling this research gap. Therefore, the objective of this study is to develop a detection model that integrates Sentinel-1 imagery, texture analysis, adaptive thresholds, and machine learning to accurately detect oil spills and verify similar phenomena in the waters of northern Bintan. These findings are expected to not only contribute to methodological advances but also support faster response times, strengthen environmental protection, and reduce economic losses due to oil spills, thereby providing additional useful information for regional maritime policy-making and management.

2. RESEARCH METHOD

2.1 Study Area and Data Collection

This research was conducted in coastal villages in the northern part of Bintan Island, as this location regularly experiences oil spills every year, specifically in the villages of Berakit, Pengudang, Sebong Lagoi, Sebong Pereh, Tanjung Uban Utara, Tanjung Uban Kota, and Malang Rapat.

This study used four data sets, namely Sentinel-1 radar imagery data, ECMWF wind data, UCSB/CHG rainfall data, and NOAA sea surface temperature data.

Sentinel-1 Data

Sentinel-1 satellite imagery data can be retrieved from the Google Earth Engine platform under the collection name COPERNICUS/S1_GRD and instrument mode IW. For training and testing data, three images were retrieved, namely on March 3, 2021, March 16, 2022, and March 23, 2024. Meanwhile, for inference data, images from March 23, 2024, were used. In addition, images were also taken on March 29, 2024, March 12, 2025, March 18, 2025, and March 30, 2025, for additional inference data to facilitate a more comprehensive analysis process. With Sentinel-1 radar images, several features or variables can be obtained to detect oil spills, including basic features such as VV (Vertical-Vertical) and VH (Vertical-Horizontal), texture analysis features such as homogeneity / Inverse Different Moment (IDM), entropy, and Angular Second Moment (ASM), and polarization operation features such as VV+VH (Add), VV-VH (Subtract), VVxVH (Multiply), VV/VH (Divide), and (VV+VH)/2 (Average) [11], [12], [13], [14], [15].

Wind Data

The wind data used comes from the ECMWF (European Center for Medium-Range Weather Forecasts) via the Google Earth Engine platform using the ECMWF/ERA5_LAND/HOURLY collection with the same data collection time range as the 5 inference images, so that the u and v values used in calculating wind speed (m/s) using equation 1 can be obtained [16].

$$\text{Wind speed} = \sqrt{u^2 + v^2} \tag{1}$$

Where u is the east-west wind vector component and v is the north-south wind vector component.

Rainfall data

The rainfall data used was obtained from UCSB/CHG via the Google Earth platform using the UCSB-CHG/CHRIPS/DAILY collection with the same data collection time range as the five inference images, thereby obtaining daily rainfall values (mm/day).

Sea surface temperature data

The sea surface temperature data used was obtained from NOAA via the Google Earth Engine platform using the NOAA/CDR/OISST/V2_1 collection with the same data collection time range as the 5 inference images. After that, the raw data was calibrated to convert the integer scale to degrees Celsius, resulting in the final sea surface temperature value (°C).

2.2 Data Labeling

The labeling process was carried out on Sentinel-1 satellite image data using the adaptive thresholding method in a 100-pixel window and an offset value of 3.5 dB via the Google Earth Engine. Both parameters were selected as they correspond to the characteristics of oil spills, which generally exhibit lower backscatter values and

smoother surface textures compared to surrounding seawater. That parameter value were also used by Maryanto & Nurohman (2024) [17]. Oil spill detection with SAR data is based on the nature of oil, which dampens the roughness of the sea surface, resulting in a dark spot due to low backscatter values. Dark spots can be detected using the adaptive thresholding method through Google Earth Engine. The results of oil spill area detection using this method will then be compared with VV polarization images. If the patterns and spots of the oil spill are similar, they can be used for the labeling process [17], [18].

2.3 Data Preparation

At this stage, data preparation is carried out for all datasets that have passed the data understanding stage. This stage includes SAR data pre-processing, which covers data subsetting, unit conversion, speckle filtering, and normalization via the Google Earth Engine. Unlike many conventional datasets, missing values are not a major issue in satellite imagery, as all pixels will be available during the image recording process on the desired date. Therefore, handling missing data is not necessary. Instead, the main challenge lies in data quality issues, such as speckle noise or environmental conditions that can affect the accuracy of oil spill detection. This is explained in detail as follows:

Subsetting Data

At this stage, radar images are cropped according to the Area of Interest (AOI) via the Google Earth Engine, so that the data analyzed only covers the research area. This allows for faster data processing, as it avoids processing data outside the study area that is not relevant to the research [19]. This process is carried out using Google Earth Engine by manually forming polygons according to the area to be studied or the research locus.

Unit Conversion

Unit conversion is performed from the decibel (dB) scale to the linear scale via the Google Earth Engine, so that the analysis process can be carried out more comprehensively. This needs to be done because a difference of 1 unit on the decibel scale does not represent a consistent absolute change, but rather a logarithmic relative change, which can minimize variation and hide important patterns. The equation for performing unit conversion can be seen in equation 2 [20].

$$\text{Linear backscatter} = 10^{\frac{\text{decibel backscatter}}{10}} \quad (2)$$

Speckle Filtering

This stage aims to reduce or even eliminate the influence of atmospheric disturbances such as dust particles so that the images are clearer and more distinct for further study. This stage is carried out through Google Earth Engine using the Lee Filter and a window size of 50 meters in the form of a circle [21], [22].
Speckle Filtering

Normalization

Normalization is performed so that all variables have a range of values that are not too different from each other, allowing for more accurate interpretation and analysis. In this study, the normalization method used is min-max normalization using Google Colab, as it is the most common method in image data processing. This normalization is applied by reducing the value of each feature/variable by the minimum value of each feature/variable and then dividing it by the range of values of that feature/variable [23].

2.4 Modeling

The entire modeling process was conducted using the Google Colab, which provides a cloud-based environment with GPU acceleration to facilitate efficient computation and training. Some of the machine learning algorithms used in searching for the best model include Support Vector Machine (SVM), K-Nearest Neighbor (KNN), Gaussian Naïve Bayes (GNB), Gaussian Mixture Model (GMM), Linear Discriminant Analysis (LDA), Random Forest (RF), and Extreme Gradient Boosting (XGBoost). Meanwhile, deep learning algorithms such as Convolutional Neural Network (CNN) and Long Short-Term Memory (LSTM) are also used in the search for the best model or algorithm. Then, the grid search method is used to find the best parameters for each algorithm so that the results obtained can be more optimal. In addition, computation time is also taken into account when selecting the best model.

Each model was evaluated using cross-validation — 10-fold for machine learning algorithms, 5-fold for CNN, and 3-fold for LSTM — with performance metrics derived from the confusion matrix, including precision, recall, accuracy, and F1-score. After determining the best model, model optimization is carried out so that the evaluation results and detection results can work optimally. Model optimization can be done in various ways, such as parameter tuning, feature engineering, threshold optimization, class balancing with SMOTE, and so on. Once the model performance has improved, the best model for detecting oil spills has been obtained.

2.5 Look-alike Identification

If the detection results are accurate, the research can proceed with the process of identifying look-alike oil spills. Look-alike oil spills on radar images can be natural surfactants produced by phytoplankton or fish, rain, and areas with low wind speeds. Look-alike oil spills can be found in water areas with sea surface temperatures reaching 22°C – 26°C, rainfall of ≥0 mm/day, and wind speeds below 2 m/s or above 14 m/s. Meanwhile, on land, the process of identifying look-alike oil spills can be done through Google Street View [19], [24], [25].

2.6 Area Calculation

The next step is to calculate the area of the oil spill and look-alikes using Google Colab by multiplying the number of pixels that meet the criteria by the square of the pixel resolution used in the study, which is 7 meters. This is because each pixel in the projected image represents a certain area, which can be referred to as spatial resolution [18].

3. RESULT AND ANALYSIS

3.1 Oil Spill Detection

Oil spill detection can be done in various ways, such as fixed thresholding, adaptive thresholding, GLCM (Gray Level Co-Occurrence Matrix) texture analysis, machine learning model creation, and so on. However, this study will use an adaptive thresholding approach, as well as the creation of the best models from machine learning and deep learning using grid search and several features, including GLCM texture features.

Adaptive Thresholding

Adaptive thresholding was applied by calculating the average backscatter within a 100-pixel window. This was followed by calculating the adaptive threshold based on the average backscatter and an offset value of 3.5 dB. Finally, dark spots with backscatter lower than the adjusted threshold were identified as oil spills in the red area and can be seen in Figure 1b. The results are similar to the VV polarization image in Figure 1a, so they can be used in the labeling process.

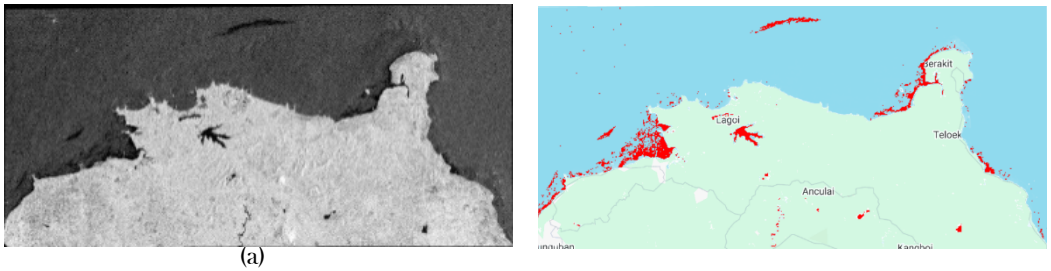

(a) (b)

Figure 1. Image visualization. (a) VV polarization. (b) Results of the adaptive thresholding method.

Modeling

Modeling was performed by dividing the training and testing data in a ratio of 70% and 30%, respectively. The results of the performance evaluation of each algorithm are shown in Table 1.

Table 1. Evaluation results of each algorithm

Algorithm	Measure Evaluation				Computational Time (s)
	Accuracy	Precision	Recall	F1-Score	
SVM	0.8661	0.8745	0.8661	0.8692	896.30
KNN	0.8692	0.8676	0.8692	0.8681	35.50
GMM	0.8203	0.8270	0.8203	0.8233	13.53
GNB	0.8406	0.8432	0.8406	0.8385	1.03
LDA	0.4289	0.2179	0.4289	0.2890	1.32
RF	0.8683	0.8697	0.8683	0.8688	1692.25
XGBoost	**0.8700**	**0.8698**	**0.8700**	**0.8696**	**345.91**
CNN	0.8667	0.8642	0.8667	0.8639	3602.39
LSTM	0.8598	0.8586	0.8598	0.8590	7360.04

It can be seen that the XGBoost algorithm has the best evaluation results when compared to other algorithms. This model also shows no significant signs of overfitting, as indicated by the training data accuracy of 0.8890 with only a 0.0190 difference from the testing data accuracy. Although its computational time is not the shortest, 345.91 seconds is considered relatively efficient given the model's strong performance. The next step is to apply this model to the inference image (March 23, 2024), which can be seen in Figure 2.

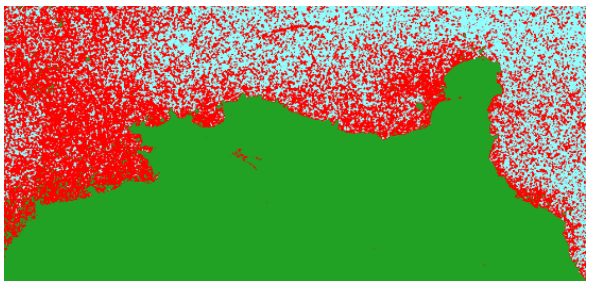

Figure 2. Mapping oil spills with the XGBoost model.

It can be clearly seen that the classification results are overestimated when compared to the visualization of oil spills using the adaptive thresholding method in Figure 1b. This is because the frequency distribution of each label in the data used for training and testing is almost the same. Meanwhile, in the inference image, the frequency of class 1 (oil) is much less than the other two classes. Therefore, it is necessary to re-model with new data, so that the evaluation results of each algorithm model with new data can be obtained in Table 2.

Table 2. Evaluation results of each algorithm with new data

Algorithm	Measure Evaluation				Computational Time (s)
	Accuracy	Precision	Recall	F1-Score	
SVM	0.9289	0.9730	0.9289	0.9473	4042.38
KNN	0.9765	0.9723	0.9765	0.9732	112.65
GMM	0.9678	0.9526	0.9678	0.9602	29.94
GNB	0.9668	0.9711	0.9668	0.9688	1.16
LDA	0.5437	0.3634	0.5437	0.4015	1.87
RF	0.9764	0.9720	0.9764	0.9732	5905.24
XGBoost	**0.9772**	**0.9733**	**0.9772**	**0.9739**	737.12
CNN	0.9762	0.9720	0.9762	0.9709	8738.16
LSTM	0.9771	0.9731	0.9771	0.9737	21563.83

It can be seen that the XGBoost algorithm has the best evaluation results when compared to other algorithms. This model also shows no signs of significant overfitting. This can be seen from the accuracy value in the training data of 0.9798 with a difference of 0.0026 from the accuracy value in the testing data. The evaluation results for each data set can also be seen in the confusion matrix in Figure 3.

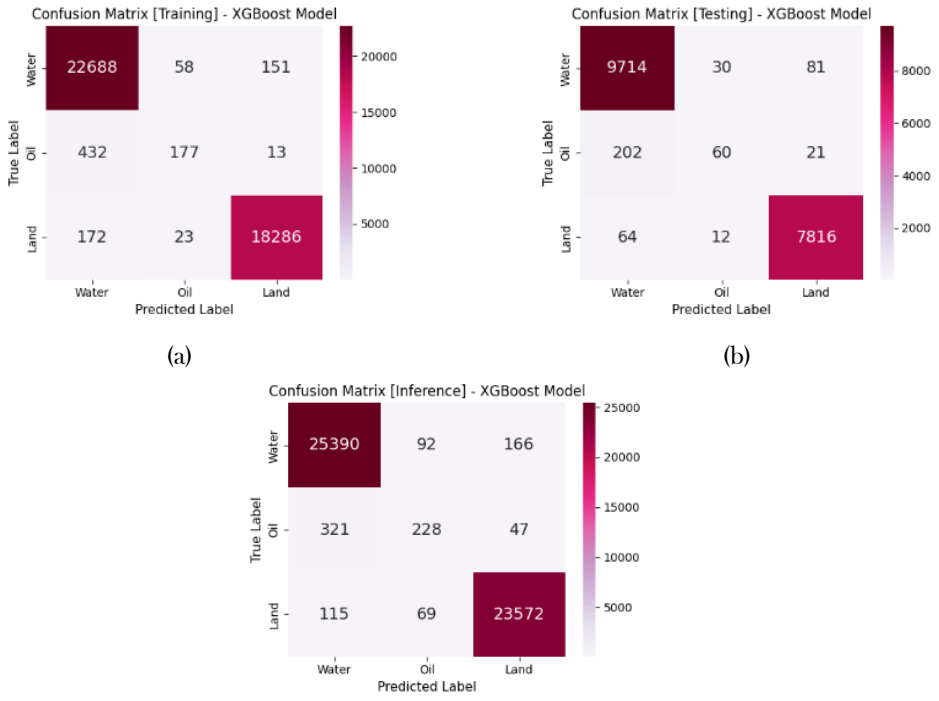

Figure 3. Confusion matrix with new data. (a) Training data. (b) Testing data. (c) Inference data.

Based on the confusion matrix above, it can be seen that the model is still not good enough in classifying class 1 (oil). This may be because the model cannot learn class 1 as much as other classes due to significant frequency differences. Therefore, model optimization needs to be carried out by reducing the VH variable, based on its lack of ability to detect oil. In addition, data imbalance was handled using SMOTE, which was 4 times greater in class 1 (oil). This was followed by hyperparameter tuning and searching for the optimal threshold value. The best threshold obtained was 0.4108, and the model evaluation results can be seen in Table 3.

Table 3. The results of evaluating each algorithm with new data in each dataset

Data	Measure Evaluation			
	Accuracy	Precision	Accuracy	F1-Score
Training	0.9701	0.9681	0.9701	0.9689
Testing	0.9690	0.9666	0.9690	0.9676
Inference	0.9796	0.9798	0.9796	0.9796

In general, it can be seen from the evaluation results in each data set that the model is quite good at classifying pixels into each class. In addition, there is no indication of overfitting, as seen from the training data accuracy value of 0.9701 with a difference of 0.0011 from the test data accuracy value. Furthermore, the results of the model evaluation after optimization on each data and class can be seen in Figure 4 and Table 4. In addition, Table 4 also includes the standard deviation values obtained from cross-validation to strengthen the analysis of the model's performance stability. In creating this model, the author gave more consideration to the evaluation results on the inference data while still paying attention to the evaluation results of the training and testing data.

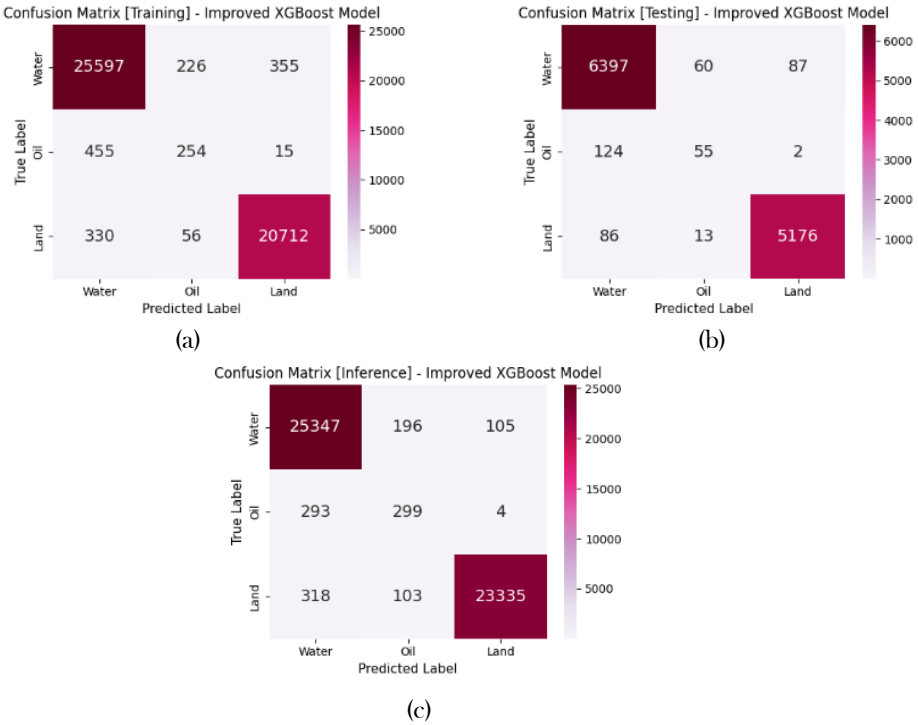

Figure 4. Confusion matrix after optimization. (a) Training data. (b) Testing data. (c) Inference data.

Table 4. Evaluation results of each algorithm after optimization

Class (Label)	Data	Measure Evaluation			
		Accuracy	Precision	Recall	F1-Score
1	Training	0.9718	0.9702	0.9778	0.9740
	Testing	0.9707	0.9682	0.9775	0.9729
	Inference	0.9821	0.9765	0.9883	0.9823
2	Training	0.9791	0.4739	0.3508	0.4032
	Testing	0.9833	0.4297	0.3039	0.3560
	Inference	0.9822	0.5000	0.5017	0.5008
3	Training	0.9773	0.9824	0.9817	0.9821
	Testing	0.9842	0.9831	0.9812	0.9822
	Inference	0.9810	0.9954	0.9823	0.9888

Based on Figure 4 and Table 4, it can be seen that the model is quite good at classifying pixels into class 1 (oil), although not as good as the other two classes, especially in the training and testing data. This can be seen in

the inference data, where the model performs reasonably well in classifying pixels into class 1 (oil), as shown in Figure 4c, where the majority of actual oil data has been classified into the correct class. This is in line with the author's objective, which is to focus more on the evaluation results in the inference data. The cross-validation results show a mean precision of 0.8532 ± 0.0415, indicating that the model achieves a fairly consistent performance across folds. The relatively low standard deviation (std = 0.0415) suggests that the model has good stability and generalizes well to data with similar characteristics. However, this model is more suitable for use in the same or similar geographical locations, as variations in environmental and oceanographic conditions can affect the distribution and characteristics of pixel values in Sentinel-1 images. Factors such as sea surface roughness, wind speed, water turbidity, and seasonal conditions can vary from region to region and can alter the backscatter response, meaning that patterns observed in one area may not necessarily apply in another. Furthermore, the analysis continued with mapping of oil spills on the inference image, as shown in Figure 5, which shows similar results to the adaptive thresholding method in Figure 1b.

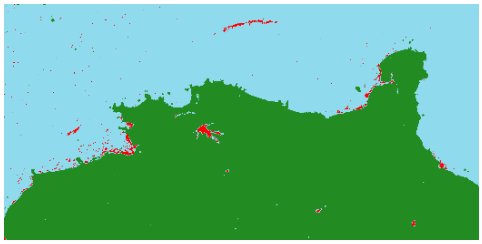

Figure 5. Mapping of oil spills with XGBoost after optimization

Next, to determine coastal areas vulnerable to oil spills, the model was applied to additional inference images, as shown in Figure 6. The image shows several areas affected by oil spills, which can help identify potentially risky areas.

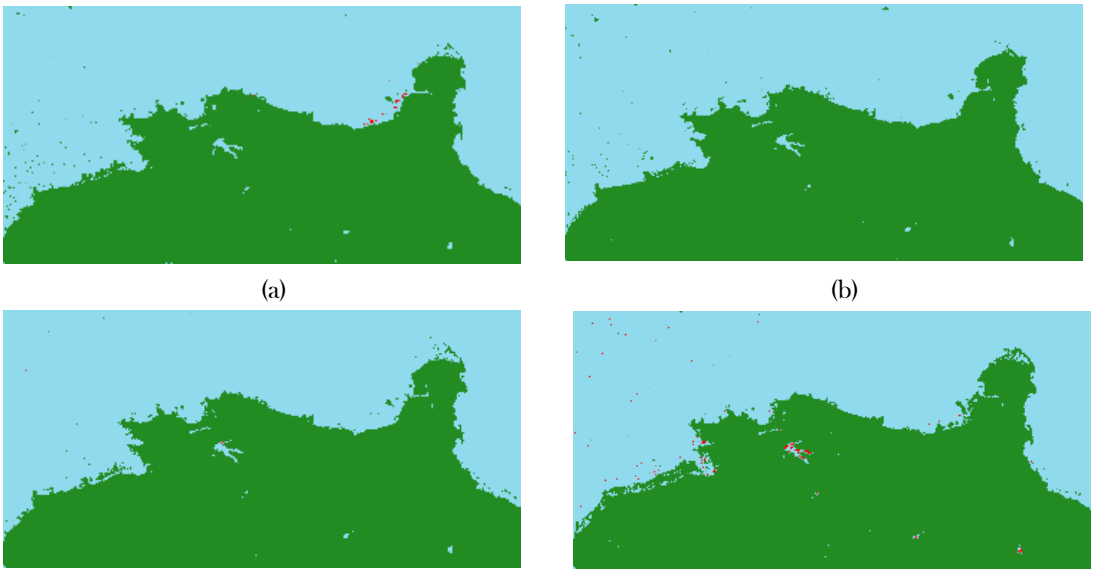

(a) (b)

(c) (d)

Figure 6. Mapping of oil spills on additional inference images. (a) March 29, 2024. (b) March 12, 2025. (c) March 18, 2025. (d) March 30, 2025.

3.2 Look-alike Identification

The next step is to reconfirm the areas that have been detected as oil spills through the process of identifying look-alike oil spills. Before identifying look-alike oil spills, it is necessary to divide the oil spill areas in the waters, coastal areas, and land areas into several polygons so that the analysis can be carried out more accurately. On March 23, 2024, there were five oil spill polygons in coastal, marine, and land areas. Then, on March 29, 2024, there were three oil spill polygons in coastal and marine areas. Finally, on March 12, 2025, there was only one oil spill polygon in coastal and marine areas. On March 18, 2025, there were 2 oil spill polygons, both in coastal and marine areas and on land. Then on March 30, 2025, there were 6 oil spill polygons in coastal and marine areas, and 5 polygons on land. After that, the process of identifying look-alikes in water and coastal areas can be continued using sea surface temperature (NOAA), wind (ECMWF), and rainfall (UCSB/CHG) data. The results show that almost all areas detected as oil spills in the five inference images are actual oil spills, except for the oil

spill in the coastal and water areas on March 18, 2025, which is a look-alike oil spill object. This is because it rained on the date and location of the oil spill.

Next, the analysis can be continued by identifying the suitability of conditions on land through visual observation using Google Street View. This process is carried out by reviewing locations that were previously detected as oil spill areas in the classification results, particularly in land areas that are accessible and have street view imagery available, so that the actual surface conditions can be verified visually. The results show that all areas detected as oil spills in the middle of the land are look-alike oil spill objects, with details of the objects being Lagoi Bay Lake, Bintan Resort Cakrawala Reservoir, granite mines, water reservoirs, and Kawal Bintan Reservoir. These objects were also detected as oil spills because the calm water areas in the middle of the mainland also have low backscatter, similar to oil spills.

3.3 Area Calculation

The research stages can be continued by calculating the area of the oil spill and look-alike areas, as detailed in Table 5.

Table 5. Results of calculating the area of oil spills and look-alikes

Date	Object	Area Size (m^2)	Nearest Location
23 March 2024	Oil spill	5,400,241	Trikora Beach, Bakau Terang Beach, Club Med Bintan Island, Treasure Bay Bintan, TRC Bintan Resort, Sakerah Beach.
	Oil spill look-alikes	1,333,045	Lagoi Bay Lake, Bintan Resort Cakrawala Reservoir, Granite Mine, Water Reservoir, Kawal Bintan Dam.
29 March 2024	Oil spill	414,932	Bintan Brzee Beach, Roka Resort, Club Med Island.
12 March 2025	Oil spill	6,174	Bakau Terang Beach.
18 March 2025	Oil spill look-alikes	116,326	Kawal Bintan Reservoir, Tanjung Berakit Beach, Bintan Resort Cakrawala Reservoir, Sakerah Beach.
30 March 2025	Oil spill	889,497	Trikora Beach, Bintan Exotica Resort by Waringin Hospitality, Bintan Brzee Beach, Roka Resort, Treasure Bay Bintan, TRC Bintan Resort, Hamid Beach.

It can be seen that there are several coastal areas where oil spills are frequently found, such as Bakau Terang Beach, Club Med Bintan Island, Trikora Beach, Roka Resort, Bintan Brzee Beach, Treasure Bay Bintan, and TRC Bintan Resort. Therefore, these coastal areas should be noted by the government and local communities as coastal areas that are prone to oil spills, in order to increase preparedness in dealing with oil spill problems that are routinely found every year. These findings also highlight the potential environmental risks to local ecosystems such as mangroves and coral reefs, which serve as important habitats for marine life. The spatial identification of these vulnerable areas can assist local authorities in prioritizing response actions, strengthening monitoring systems, and formulating preventive policies to mitigate recurring oil spill incidents.

4. CONCLUSION

Based on the research results, it can be concluded that the best model for oil spill detection in the northern waters of Bintan Island is the XGBoost algorithm after optimization with the highest evaluation results in terms of accuracy and recall. In addition, further analysis is needed so that the detection results can be more accurate using additional data to identify look-alike oil spills. As a result, seven locations were identified as areas prone to oil spills and five locations were identified as areas prone to look-alike oil spills. This model can also be applied to detect daily oil spills using radar images in the northern part of Bintan Island at times other than those used in this study.

Furthermore, the Ministry of Environment and Forestry (KLHK), particularly through the Directorate General of Pollution and Environmental Damage Control (PPKPL), can utilize the daily oil spill detection model developed in this study as an effort to monitor and control coastal and marine pollution. In addition, the information on coastal areas identified as vulnerable to oil spills can serve as a basis for decision-making in managing and mitigating environmental damage in marine areas.

In addition, this study has limitations in identifying relevant variables in creating an oil spill detection model, particularly when using radar imagery. This is because the majority of previous studies have used optical imagery. For future research, it is hoped that other more relevant variables can be found in line with scientific developments and that comparisons can be made between detection results using radar and optical imagery. Overall, this study provides a methodological contribution by integrating texture analysis, adaptive thresholding, and the XGBoost algorithm for Sentinel-1-based oil spill detection, while also offering new regional insights into oil spill vulnerability in the northern waters of Bintan Island.

5. REFERENCES

[1] M. A. Z. F. Najwa Tiara Maharani, Agus Setiawan, "Modeling oil spills in the waters of the Riau Islands using NOAA oil modeling environment (GNOME) software," (in Indonesian), *J. Ilmu Kelaut. Kepul.*, vol. 5, no. 1, pp. 571–584, doi: 10.33387/jikk.v5i1.4856.

[2] S. Rahmawati, R. K. Agustini, and A. Efritadewi, "Analysis of the impact and response to oil spills in Bintan Waters," (in Indonesian), *Aufklarung J. Pendidikan, Sos. dan Hum.*, vol. 3, no. 4, pp. 1–8, [Online]. Available: http://pijarpemikiran.com/index.php/Aufklarung

[3] R. Duha, V. Mardianti, and Z. R. Ramadhani, "Implementation of UNCLOS 1982 in addressing marine pollution by the Indonesian Government: a case study of oil pollution in the border area of Bintan Regency," (in Indonesian), *Konstitusi J. Hukum, Adm. Publik, dan Ilmu Komun.*, vol. 1, no. 4, pp. 274–286, doi: 10.62383/konstitusi.v1i4.229.

[4] Kementerian Energi dan Sumber Daya Mineral Republik Indonesia, *Keputusan Direktur Teknik dan Lingkungan Minyak dan Gas Bumi selaku Kepala Inspeksi No.21.K/MG.06/DMT/2022 tentang Pedoman dan Tata Cara Pelaporan Keselamatan Minyak dan Gas Bumi*. Indonesia, 2022, p. 41. [Online]. Available:https://migas.esdm.go.id/cms/uploads/regulasi/2024/a3bde38d94aca2e0db7478d6bde86456.pdf .https://migas.esdm.go.id/cms/uploads/regulasi/2024/a3bde38d94aca2e0db7478d6bde86456.pdf

[5] Direktorat Jenderal Pengendalian Pencemaran dan Kerusakan Pesisir dan Laut KLHK, "Laporan kinerja 2024," Jakarta, 2024. [Online]. Available: https://ppkl.menlhk.go.id/website/filebox/1017/250224112700LKj Ditjen PPKL 2024_FINAL.pdf

[6] Direktorat Jenderal Pengendalian Pencemaran dan Kerusakan Pesisir dan Laut KLHK, "Laporan kinerja tahun 2023," Jakarta, 2023. [Online]. Available: https://ppkl.menlhk.go.id/website/filebox/1204/240125134444LKJ PPKPL 2023 (1).pdf

[7] Direktorat Jenderal Pengendalian Pencemaran dan Kerusakan Pesisir dan Laut KLHK, "Laporan kinerja tahun 2022," Jakarta, 2022. [Online]. Available: https://ppkl.menlhk.go.id/website/filebox/1179/230830095445LKJ PPKPL 2022.pdf

[8] K. I. Suniada, "Utilization of Sentinel-1 satellite imagery data for monitoring oil spill distribution in WPP 713," (in Indonesian), *J. Kelaut. Nas.*, vol. 16, no. 1, pp. 15–24, 2021, doi: 10.15578/jkn.v16i1.9293.

[9] R. Prastyani and A. Basith, "Detection of oil spills in the Makassar Strait using active and passive remote sensing sensors," (in Indonesian), *J. Geod. dan Geomatika*, vol. 2, no. 1, pp. 88–94, 2019, doi: 10.14710/elipsoida.2019.4864.

[10] S. Najafizadegan and M. Danesh-Yazdi, "Variable-complexity machine learning models for large-scale oil spill detection: The case of Persian Gulf," *Mar. Pollut. Bull.*, vol. 195, no. July, p. 115459, 2023, doi: 10.1016/j.marpolbul.2023.115459.

[11] M. Az-zahra, A. S. Handayani, and L. Lindawati, "Comparison of VV and VH polarity in the application of the NDFI algorithm in flood mapping of Palembang City," (in Indonesian), *J. Teknol. Sist. Inf. dan Apl.*, vol. 7, no. 1, pp. 10–18, 2024, doi: 10.32493/jtsi.v7i1.36209.

[12] A. Saragih and M. Sianturi, "Implementation of the color moment and GLCM methods for detecting rubber leaf disease," (in Indonesian), *Inf. dan Teknol. Ilm.*, vol. 7, no. 2, pp. 145–151, 2020, [Online]. Available: https://ejurnal.stmik-budidarma.ac.id/inti/article/view/2377.

[13] Z. Y. Lamasigi, "DCT for GLCM-based feature extraction in batik identification using K-NN," (in Indonesian), *Jambura J. Electr. Electron. Eng.*, vol. 3, no. 1, pp. 1–6, 2021, doi: 10.37905/jjeee.v3i1.7113.

[14] S. Santosa, Martono, M. B. Utomo, and B. S. Budi, "Selection of computational angle direction and GLCM features in image extraction of teak, mahogany, mindi, and sengon wood," (in Indonesian), *J. Wahana Tek. Sipil*, vol. 23, no. 2, pp. 77–87, 2018, doi: 10.32497/wahanats.v23i2.1363.

[15] P. M. Afgatiani, A. G. Suhadha, and A. Ibrahim, "The capability of Sentinel-1 polarization combinations for oil spill detection (study case: Karawang, Indonesia)," *IOP Conf. Ser. Earth Environ. Sci.*, vol. 1109, no. 1, pp. 1–8, 2022, doi: 10.1088/1755-1315/1109/1/012078.

[16] N. D. Pratiwi, Muliadi, and Risko, "Estimated significant wave height on the coast of Sengkubang Mempawah, West Kalimantan," (in Indonesian), *Oseanologia*, vol. 3, no. 1, pp. 8–16, 2023, doi: 10.26418/jose.v3i1.77583.

[17] T. I. Maryanto and R. Nurohman, "Identification of oil spills and prediction of their spread based on interpretation of Sentinel-1A imagery in the waters of Karawang, West Java," (in Indonesian), *Berk. Perikan. Terubuk*, vol. 52, no. 2, pp. 2240–2250, 2024, [Online]. Available: https://berkalaterubuk.com/index.php/terubuk/article/view/2/2.

[18] B. H. Husain, "Illegal Oil Discharge (Oil Bilge) Monitoring Application Using Sentinel 1A Synthetic Aperture Radar Satellite Data Broadcast and Automatic Identification System (AIS) for Ships in the Sunda Strait, Banten Province," (in Indonesian), *Maj. Suligi*, vol. 11, no. 24, pp. 1–6, 2022, doi: 10.24843/JIM.2018.v06.i03.p11.

[19] D. H. Santoso, "Study of Water Carrying Capacity on Bintan Island, Riau Islands Province," (in Indonesian), *J. Sains & Teknologi Lingkung.*, vol. 7, no. 1, pp. 01–17, 2015, doi: 10.20885/jstl.vol7.iss1.art1.

[20] Esri, "Convert SAR units (image analyst)," ArcGIS Pro. [Online]. Available: https://pro.arcgis.com/en/pro-app/3.3/tool-reference/image-analyst/convert-sar-units.html.
[21] S. Sulma, K. I. N. Rahmi, N. Febrianti, and J. Sitorus, "Oil spill detection using adaptive thresholding and texture analysis on SAR data," (in Indonesian), *Maj. Ilm. Globe*, vol. 21, no. 1, pp. 45–52, 2019, doi: 10.24895/MIG.2019.21-1.925.
[22] P. Kupidura, "Comparison of filters dedicated to speckle suppression in SAR images," (in Indonesian), *Int. Arch. Photogramm. Remote Sens. Spat. Inf. Sci. - ISPRS Arch.*, vol. 41, no. July, pp. 269–276, 2016, doi: 10.5194/isprsarchives-XLI-B7-269-2016.
[23] B. G. Chepino, R. R. Yacoub, A. Aula, M. Saleh, and B. W. Sanjaya, "Effect of minmax normalization on ORB data for improved ANN accuracy," *J. Electr. Eng. Energy, Inf. Technol.*, vol. 11, no. 2, p. 29, 2023, doi: 10.26418/j3eit.v11i2.68689.
[24] B. Nababan, E. G. B. Sihombing, and J. P. Panjaitan, "Variability of sea surface temperature and chlorophyll-a concentration in the Northeast Indian Ocean, West Sumatra," (in Indonesian), *J. Teknol. Perikan. dan Kelaut.*, vol. 12, no. 2, pp. 143–159, 2021, doi: 10.24319/jtpk.12.143-159.
[25] M. Alviriza Ramadhan, F. Tri Anggraeny, and C. Aji Putra, "Classification of daily rainfall using the K-Nearest Neighbor method," (in Indonesian), *JATI (Jurnal Mhs. Tek. Inform.*, vol. 8, no. 3, pp. 3863–3869, 2024, doi: 10.36040/jati.v8i3.9817.